After benzidine reaction, sections were counterstained with hematoxylin. Negative controls were done by substitution of the primary antibodies with nonimmunized serum.

Semiquantitative assessment of immunohistochemical results and statistics

The intensity of immunostaining of iNOS and eNOS in splenic sinuses was assessed by the following grading scale: − to ±, absent or minimal; 1+, weak; 2+, moderate; and 3+, strong. The number of ET-1-positive cells was quantitatively determined; that is, the number of ET-1-positive cells in the red pulp was counted in a blinded fashion at a magnification of ×200 under the light microscope, and the total cell number was calculated for 10 high-power fields (HPFs). Histological evaluation was performed by two independent pathologists (Y. S. and S. S.).

The mean and standard deviation (SD) were calculated for the parameters determined. Statistical significance was evaluated using Student's t test, Fisher's exact probability test, or Sperman rank correlation test. All data analyses were performed using the Statview-J5.0 software application (Abacus Concepts, Inc., Berkley, CA). P values <0.05 were considered statistically significant.

Results

Histology of the spleen

Spleens of IPH and LC showed fibrocongestive changes (Fig. 1), composed of fibrous thickening of the capsule and fibrosis and expansion of the red pulp (Table 2). White pulp follicles were generally inconspicuous. In two cases of IPH and three cases of LC, the white pulp follicles were well preserved, and the density of the white pulp area appeared to vary from case to case. Accumulations of hemosiderin-laden macrophages were occasionally seen, and sclerosiderotic nodules (Gamna-Gandy bodies) were present in three cases.

The most striking feature of IPH spleen was dilatation of the sinuses (Figs. 1A and 1B). The sinus dilatation in IPH was characterized by irregularly enlarged slits of the sinuses and irregularly formed and proliferated endothelial cells. Compared with these histological features of IPH, the slits between sinus endothelial cells tended to be narrow and almost uniform in LC spleens (Fig. 1C). Control spleens generally showed the normal structure, with narrow and regular sinuses and endothelial cells arranged parallel to the long axis of the sinus (Fig. 1D). Such sinus dilatation was more frequent in IPH compared to LC and controls ($P < 0.05$ by Fisher's exact probability test) (Table 2). No acute splenitis was observed in any case examined.

Expression of iNOS

Expression of iNOS was seen on the sinus lining cells of the red pulp. In IPH, expression of iNOS in sinus lining cells was diffuse and strong (Figs. 2A and B). In comparison with IPH, the intensity was apparently weak in LC spleens (Fig. 2C) and faint or negligible in control spleens (Fig. 2D). In addition, iNOS was expressed weakly and focally on the endothelium of the artery branches at the hilus to the arterioles (penicilliary arteries), and also in the endotherium of the veins, and the frequency and intensity of iNOS expression were not significantly different in these vessels among the three groups. A few scattered polymorphonuclear and mononuclear leukocytes in the red pulp also weakly expressed iNOS in all three groups.

Expression of eNOS

Similarly to iNOS immunostaining, eNOS was mainly expressed on sinus lining cells of the red pulp. Interestingly, eNOS was strongly expressed on sinus lining cells of IPH spleens (Figs. 3A and B) and, to a lesser degree, of LC spleens (Fig. 3C). The eNOS immunoreactivity of sinus lining cells was faint or negligible in the control group (Fig. 3D). Additionally, eNOS was weakly expressed on the endothelium along the vascular tree of the arteries and veins of the spleens in the IPH, LC, and control groups. Expression of eNOS could not be detected in leukocytes in the red pulp or white pulp in any group.

Expression of ET-1

In IPH and controls, ET-1 was expressed in the cytoplasm of scattered mononuclear leukocytes in the red pulp (Figs. 4A, 4B, and 4D). In LC spleens, a few mononuclear leukocytes in the red pulp showed positive signals for ET-1 (Fig. 4C). While the number of ET-1-positive cells in the red pulp was low in LC spleens, they were relatively dense in comparison with IPH and controls.

Semiquantitative assessment

The intensity and extent of immunohistochemical expression of iNOS and eNOS in sinus lining cells of the spleens were more intense and extensive in IPH than in LC and controls ($P < 0.05$, Sperman rank correlation test) (Figs. 5A and B). As for ET-1 immunostaining, the number of ET-1-positive cells in the red pulp was increased in LC spleens, and the increase was statistically significant compared with those in the IPH and control groups by Student's t test (Fig. 5C). No significant difference was observed in the number of ET-1-positive cells between the IPH and the control groups.

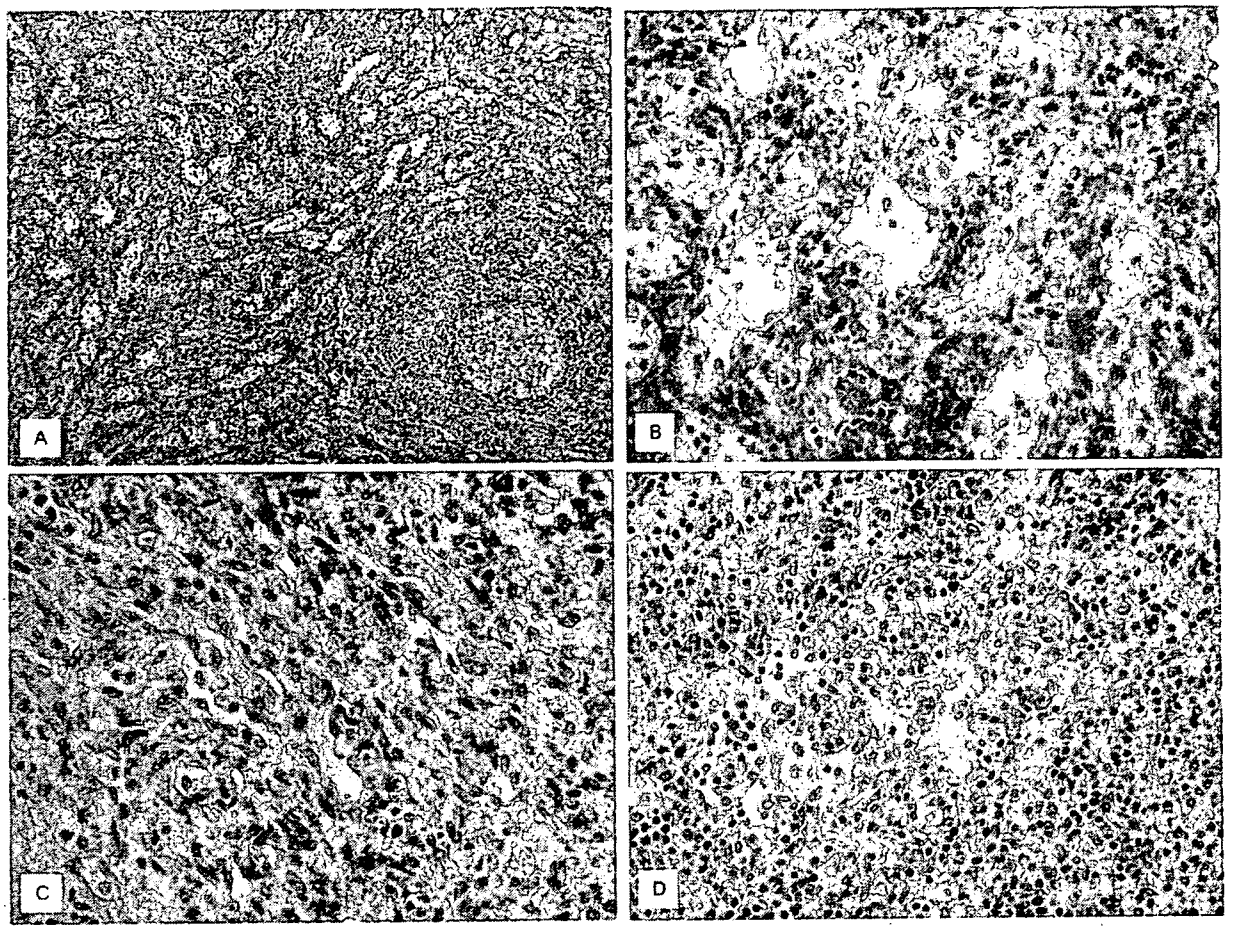

Fig. 1 Low magnification of spleens of idiopathic portal hypertension (IPH; A) and high-power view of the red pulp of IPH (B), liver cirrhosis (LC; C), and controls (D). Fibrosis and expansion of the red pulp are seen in IPH (A). In IPH, diffuse sinus dilatation of the red pulp is evident (A, B), while the slits between sinus endothelial cells are almost uniform in LC (C). (Periodic acid-Schiff. Original magnifications: A, ×100; B-D, ×400.)

Discussion

It was found in this study that iNOS and eNOS were strongly and diffusely expressed on sinus lining cells of IPH spleens. Both iNOS and eNOS are known to synthesize NO, which then works as a potent vasodilator. NO acts on the vascular cells by directly stimulating soluble guanylate cyclase, leading to increased levels of cyclic guanosine monophosphate and, consequently, decreased intercellular Ca^{2+} concentrations and thus vasorelaxation [12]. It seems conceivable that the overexpression of iNOS and eNOS in sinus endothelial cells of IPH spleens causally relates to the widespread dilatation and probably proliferation of splenic sinuses, leading to massive splenomegaly. This may in turn result in increased portal venous blood flow to the liver, thereby contributing to portal hypertension in IPH.

Previous histometric studies have showed that sinus hyperplasia and dilatation in IPH are important factors in the enlargement of the spleen [17, 18]. In IPH, the microvascular architecture of the red pulp shows the characteristic structure, which is reportedly different from that of LC. Maesawa *et al.* [8] emphasized that the interendothelial slits

Table 2 Histological features of the red pulp of the spleen

Note. IPH, idiopathic portal hypertension; LC, liver cirrhosis. $P < 0.05$ vs. [a]IPH and LC value and vs. [b]IPH and control value in this column (Fisher's exact test).

	Fibrosis	Sinus endothelial cells	Widespread sinus dilatation (>40 μm)		Gamna-Gandy body	
			Present	Absent	Present	Absent
IPH ($n = 10$)	Present	Irregularly proliferated	7	3[a,b]	2	8
LC ($n = 10$)	Present	Uniform	2	8[a]	1	9
Control ($n = 20$)	Absent	Uniform	1	19[b]	0	20

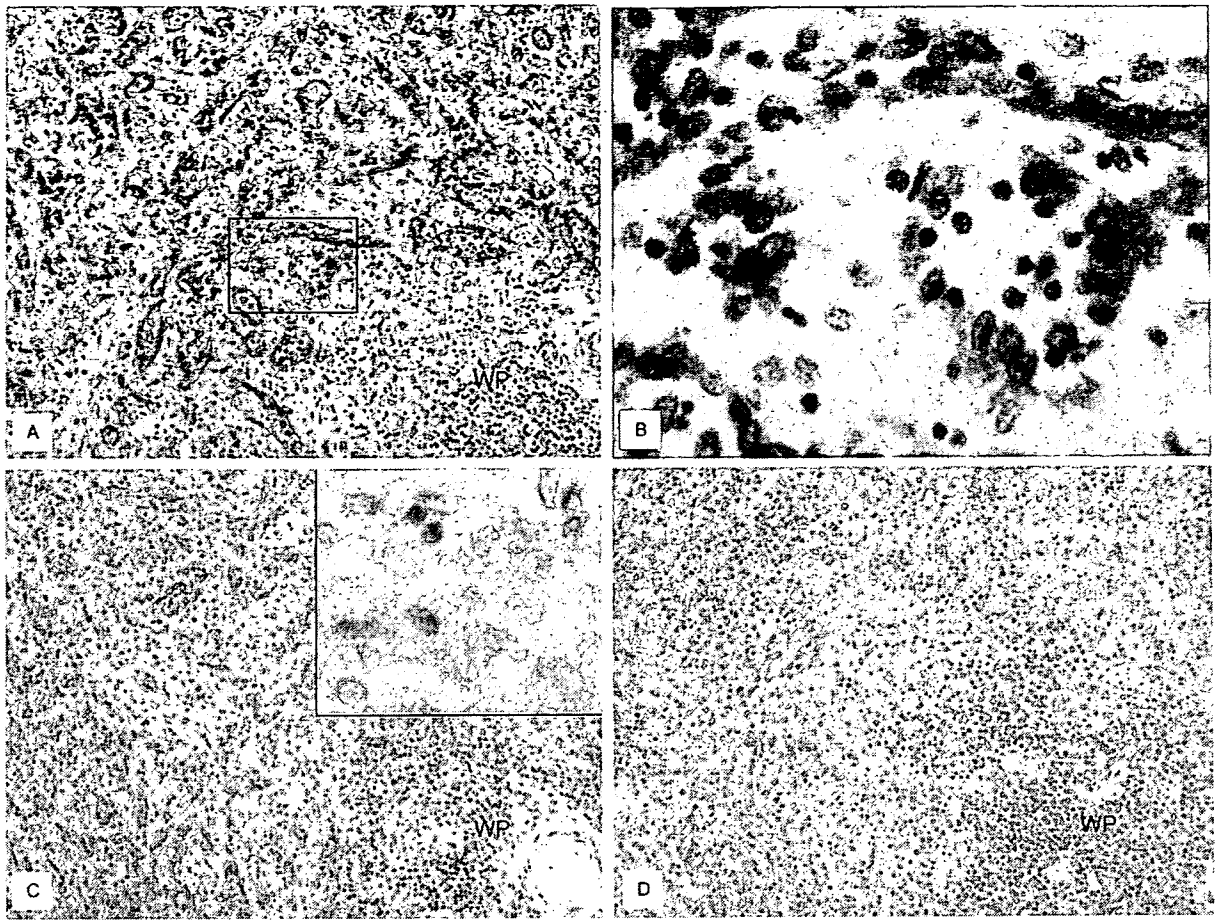

Fig. 2 Strong immunoreactivity of inducible nitric oxide synthese (iNOS) on sinus lining cells of the spleen of idiopathic portal hypertension (IPH; A and B). The staining intensity of sinus lining cells is rather weak in liver cirrhosis (LC; C) and faint or negligible in controls (D). B is a high-power view of the square outlined in A. Inset in C is a high-power view of the red pulp of LC. WP, white pulp. (Original magnifications: A, C, and D, ×200; B and C [inset], ×1000.)

of sinuses were irregulary enlarged in IPH, and proliferating cell nuclear antigen-positive sinus endothelial cells were increased in number in IPH compared with LC. In contrast, there is a report that the changes in IPH and LC spleens are essentially similar and differ only quantitatively [19]. Our data suggest that sinus endothelial cells of IPH, by overexpressing NO, contribute actively to the development of marked splenomegaly and then the maintenance of portal hypertension.

The diameter of the portal vein trunk is usually increased in IPH. Overexpression of iNOS and eNOS in IPH spleens leads to an elevation of the NO level and the spleen-derived NO presumably released into the splenic and portal vein. One possible explanation for the vasodilatation of the portal vein trunk in IPH may be due to the spleen-derived NO. Usually, NO exerts its action locally, since the half-life of NO in biologic fluids is only about 5 s [20]. In the liver of IPH, pathological changes such as fibroelastosis, phleboscrelosis, and portal venous dilatation and obliteration in portal tracts are observed, and an increase in presinusoidal vascular resistance due to these changes is regarded to be most important in the pathogenesis of IPH [1]. At the moment, the spleen-derived NO may not directly affect the microcirculation of the liver because of its short half-life. Although there is a possibility that such pathological changes in portal tracts of the IPH liver are due secondarily to increased portal blood flow and portal pressure, the causal relationship between pathological lesions in the spleen and liver of IPH requires further study.

In this study, only a few scattered mononuclear cells in the red pulp showed positive signals for ET-1 in IPH spleens, and no significant difference was observed concerning the localization and the number of ET-1-positive cells between IPH and control groups, suggesting that spleen-derived ET-1 may not have significant local and/or systemic effects on the hemodynamics of IPH patients. According to Ohara *et al.* [16], the peripheral venous ET-1 concentration is significantly elevated in IPH patients compared with that in

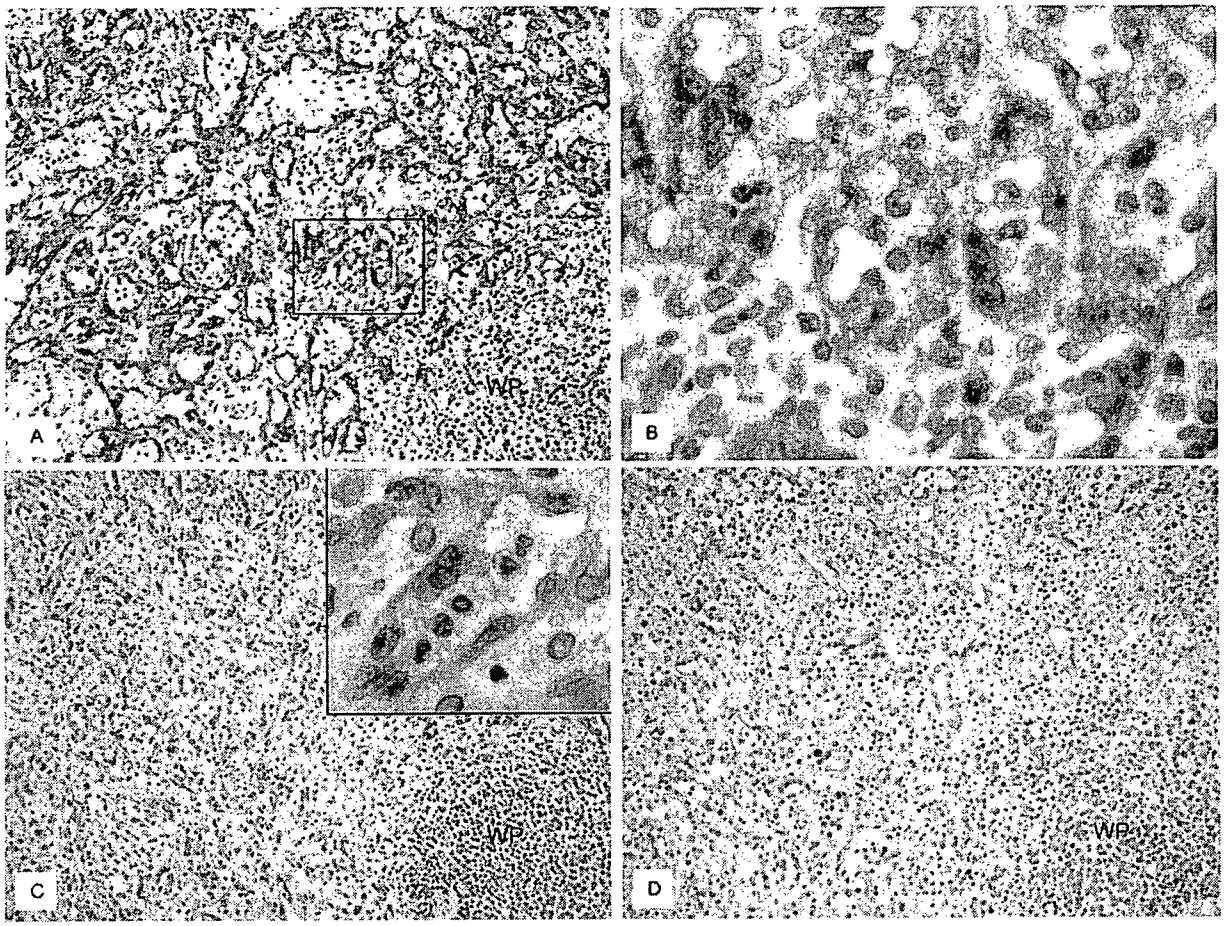

Fig. 3 Immunostaining of endothelial NOS (eNOS) for idiopathic portal hypertension (IPH; A and B), liver cirrhosis (LC; C), and control (D) spleens. Simliarly to iNOS immunostaining, strong and diffuse expression of eNOS is observed on sinus lining cells of IPH (A and B). The staining intensity of sinus lining cells is rather weak in LC (C) and faint or negligible in controls (D). B is a high-power view of the square outlined in A. The inset in C is a high-power view of the red pulp of LC. WP, white pulp. (Original magnifications: A, C, and D, ×200: B and C [inset], ×1000.)

normal controls, and the ET-1 concentration in the hepatic vein is higher than that in the peripheral vein in IPH patients. Kamath *et al.* [21] demonstrated that ET-1 was localized to periportal hepatocytes and sinusoidal cells in IPH liver. Therefore, ET-1 originating from the liver, not from the spleen, may be partially responsible for the elevation of plasma ET-1 level in patients with IPH, although the expression of ET-1 in the systemic organs of IPH patients has not yet been fully examined.

Nagasue *et al.* [15] reported that the spleen was one of the major sites of ET-1 release in cirrhotic patients, and endothelial cells of the splenic sinus and possibly B lymphocytes in the germinal center and marzinal zone of lymphoid sheaths and follicles seemed to be the sites of ET-1 production in the spleen. In this study, however, we found ET-1-positive signals in mononuclear leukocytes in the red pulp of LC spleens, and no signals for ET-1 were detected in sinus lining cells and lymphocytes in the white pulp. The reason for this contradiction is not clear at present. Although the number of ET-1-positive cells was significantly increased in the LC group compared with the IPH and control groups, the number of ET-1-positive cells was relatively low even in LC patients. Our results indicate that iNOS and eNOS, rather than ET-1, may contribute to the circulatory disturbances in LC patients, especially to the hyperdynamic circulation [22].

In summary, our data suggest that sinus lining cells of the spleens from IPH patients overexpress iNOS and eNOS, and spleen-derived NO may affect on the spleen, particularly its sinus lining cells, followed by sinus dilatation. This may in turn lead to massive splenomegaly and increased portal blood inflow to the liver, contributing to the sustained portal hypertension in IPH. Although an increase in intrahepatic, presinusoidal resistance to portal blood flow is regarded as the most important factor in the pathogenesis of IPH, a spleen-derived vasoactive substance may also be responsible

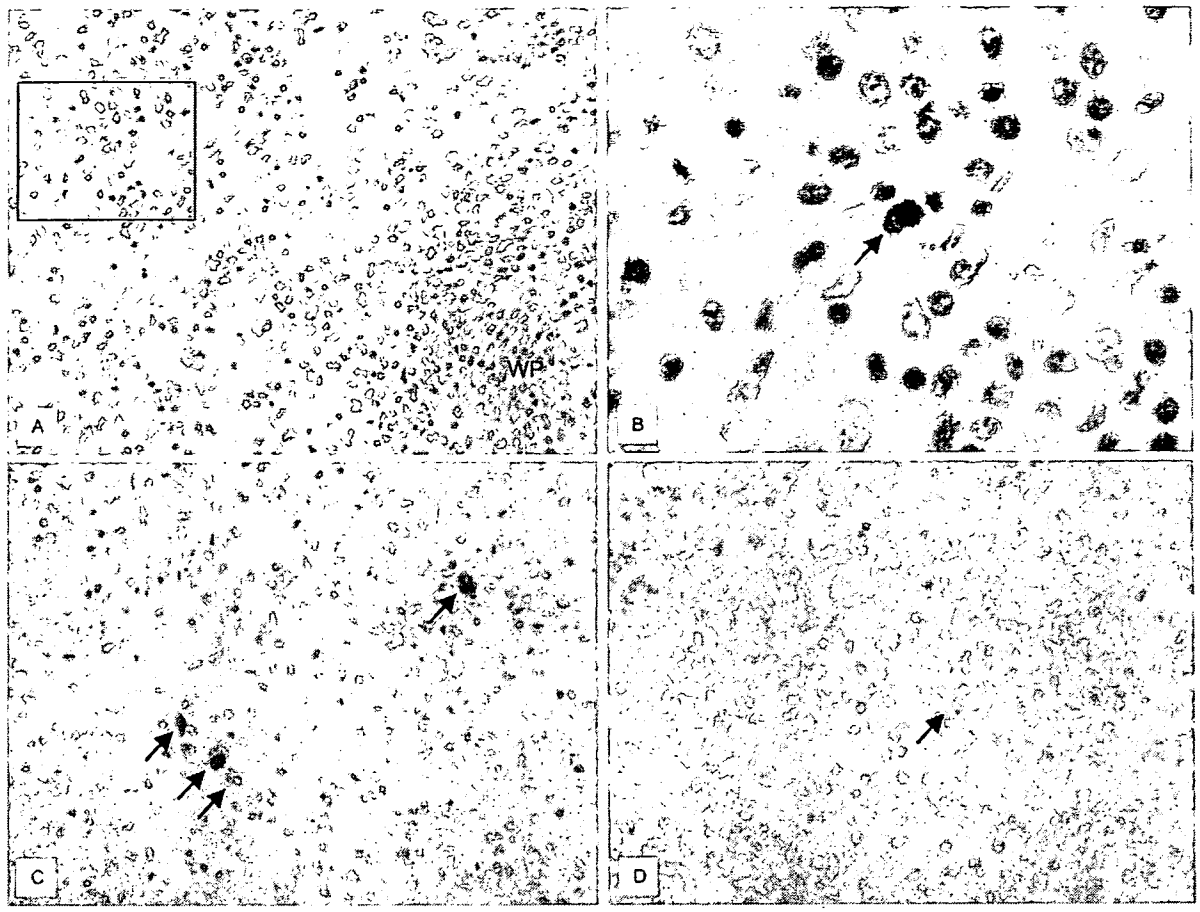

Fig. 4 Immunostaining of endothelin-1 (ET-1) for idiopathic portal hypertension (IPH; A and B), liver cirrhosis (LC; C) and control (D) spleens. C and D represent the red pulp area. ET-1-positive signals are seen scattered in mononuclear leukocytes in the red pulp. The number of ET-1-positive cells tends to be increased in LC spleens. B is a high-power view of the square outlined in A. Arrows indicate ET-1-positive mononuclear leukocytes. WP, white pulp. (Original magnifications: A, ×200; B, ×1000; C and D, ×400.)

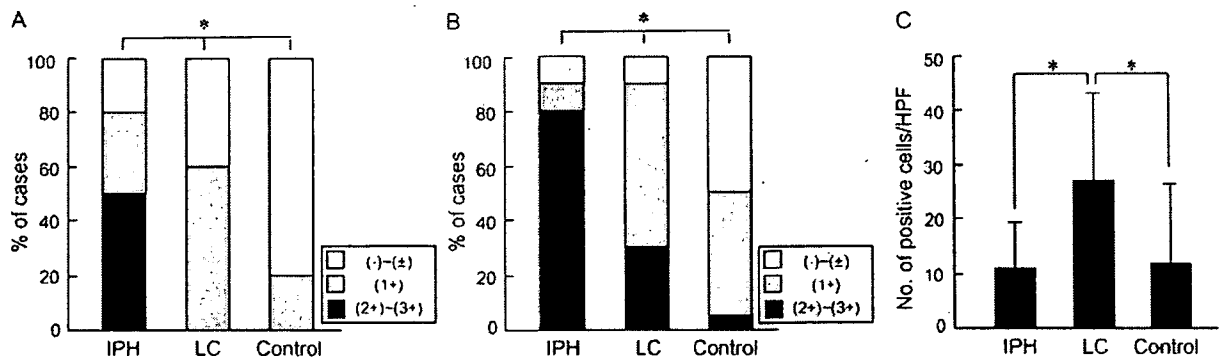

Fig. 5 Semiquantitative assessment of immunohistochemical results. The staining intensity and extent of inducible nitric oxide synthese (iNOS; A) and endothelial NOS (eNOS; B) in splenic sinuses and the number of endothelin-1 (ET-1)-positive cells (C) are shown. A significant difference is observed among the idiopathic portal hyertension (IPH), liver cirrhosis (LC), and control groups for both iNOS and eNOS expression by Sperman rank correlation test, and epression in IPH is intense and extensive. The number of ET-1-positive cells is significantly increased in LC spleens compared with IPH and control spleens by Student's *t* test. Data represent mean ± SD (C). $^{*}P < 0.05$

for IPH, and therefore, the splenomegaly of IPH seems not to be simply passive congestion.

References

1. Nakanuma Y, Tsuneyama K, Ohbu M, Katayanagi K (2001) Pathology and pathogenesis of idiopathic portal hypertension with an emphasis on the liver. Pathol Res Pract 197:65–76
2. Nakanuma Y, Hoso M, Sasaki M, Terada T, Katayanagi K, Nonomura A, Kurumaya H, Harada A, Obata H (1996) Histopathology of the liver in noncirrhotic portal hypertension of unknown aetiology. Histopathology 28:195–204
3. Okudaira M, Ohbu M, Okuda K (2002) Idiopathic portal hypertension and its pathology. Semin Liver Dis 22:59–72
4. Okuda K, Kono K, Ohnishi K, *et al.* (1984) Clinical study of eighty-six cases of idiopathic portal hypertension and comparison with cirrhosis with splenomegaly. Gastroenterology 86:600–610
5. Tsuneyama K, Ohba K, Zen Y, Sato Y, Niwa H, Minato H, Nakanuma Y (2003) A comparative histological and morphometric study of vascular changes in idiopathic portal hypertension and alcoholic fibrosis/cirrhosis. Histopathology 43:55–61
6. Tsuneyama K, Kouda W, Nakanuma Y (2002) Portal and parenchymal alterations of the liver in idiopathic portal hypertension: a histological and immunochemical study. Pathol Res Pract 198:597–603
7. Dhiman RK, Chawla Y, Vasishta RK, Kakkar N, Dilawari JB, Trehan MS, Puri P, Mitra SK, Suri S (2002) Noncirrhotic portal fibrosis (idiopathic portal hypertension): experience with 151 patients and a review of the literature. J Gastroenterol Hepatol 17:6–16
8. Maesawa C, Sakuma T, Sato T, Masuda T, Muro-oka G, Satodate R (1995) Structural characteristic of splenic sinuses in idiopathic portal hypertension. Pathol Int 45:642–648
9. Akahoshi T, Hashizume M, Tanoue K, Shimabukuro R, Gotoh N, Tomikawa M, Sugimachi K (2002) Role of the spleen in liver fibrosis in rats may be mediated by transforming growth factor beta-1. J Gastroenterol Hepatol 17:59–65
10. Kaido T, Oe H, Yoshikawa A, Okajima A, Imamura M (2004) Expressions of molecules associated with hepatocyte growth factor activation after hepatectomy in liver cirrhosis. Hepatogastroenterology 51:547–551
11. Rockey D (1997) The cellular pathogenesis of portal hypertension: stellate cell contractility, endothelin, and nitric oxide. Hepatology 25:2–5
12. Wiest R, Groszmann RJ (1999) Nitric oxide and portal hypertension: its role in the regulation of intrahepatic and splanchnic vascular resistance. Semin Liver Dis 19:411–426
13. Farzaneh-Far R, Moore K (2001) Nitric oxide and the liver. Liver 21:161–174
14. Inoue A, Yanagisawa M, Kimura S, Kasuya Y, Miyauchi T, Goto K, Masaki T (1989) The human endothelin family: three structurally and pharmacologically distinct isopeptides predicted by three separate genes. Proc Natl Acad Sci USA 86:2863–2867
15. Nagasue N, Dhar DK, Yamanoi A, Emi Y, Udagawa J, Yamamoto A, Tachibana M, Kubota H, Kohno H, Harada T (2000) Production and release of endothelin-1 from the gut and spleen in portal hypertension due to cirrhosis. Hepatology 31:1107–1114
16. Ohara N, Futagawa S, Watanabe S, Fukasawa M, Takamori S (2001) Clinical investigation of endothelin-1 and nitric oxide in patients with portal hypertension focusing on plasma levels and immunohistological staining of liver tissues. Hepatol Res 21:40–54
17. Yamamoto K (1978) Morphological studies of the spleen in splenomegalic liver cirrhosis comparing with the spleen in idiopathic portal hypertension (so-called Banti's syndrome without liver cirrhosis). Acta Pathol Jpn 28:891–905
18. Cavalli G, Re G, Casali AM, Monari P (1982) The microvascular architecture of spleen in congestive splenomegaly. A morphological-histometric study. Pathol Res Pract 174:131–146
19. Suzuki T (1972) Application of scanning electron microscopy in the study of the human spleen: three dimensional fine structure of the normal red pulp and its changes as seen in splenomegalias associated with Banti's syndrome and cirrhosis of the liver. Nippon Ketsueki Gakkai Zasshi 35:506–522
20. Moncada S, Higgs A (1993) The L-arginine-nitric oxide pathway. N Engl J Med 329:2002–2012
21. Kamath PS, Carpenter HA, Lloyd RV, McKusick MA, Steers JL, Nagorney DM, Miller VM (2000) Hepatic localization of endothelin-1 in patients with idiopathic portal hypertension and cirrhosis of the liver. Liver Transpl 6:596–602
22. Blendis L, Wong F (2001) The hyperdynamic circulation in cirrhosis: an overview. Pharmacol Ther 89:221–231

Abdominal Imaging

Published online: 7 December 2006

Abdom Imaging (2007) 32:470–474
DOI: 10.1007/s00261-006-9154-4

MR imaging of hepatocellular carcinomas with biliary tumor thrombi

Toshifumi Gabata,[1] Noboru Terayama,[1] Satoshi Kobayashi,[1] Junichiro Sanada,[1] Masumi Kadoya,[2] Osamu Matsui[1]

[1]Department of Radiology, Kanazawa University, Graduate School of Medical Science, Takara-machi, Kanazawa City, Japan
[2]Department of Radiology, Shinshu University, School of Medicine, Matsumoto City, Japan

Abstract

We retrospectively evaluate the MR imaging findings of hepatocellular carcinomas (HCC) with biliary tumor thrombi. MR imaging was performed on six patients presenting with obstructive jaundice and/or biliary hemorrhage. T1-weighted images, T2-weighted images, MR cholangiopancreatography (MRCP), and dynamic MR images were obtained. Duodenal endoscopy was performed on all cases and hepatic resection on two cases. HCCs were 1.8–10 cm in diameter (mean 5.8 cm). Biliary tumor thrombi were detected in all patients on MR imaging. Tumor thrombi showed hypointensity on T1-weighted images, hyperintensity on T2-weighted images, and contrast enhancement on the early phase of dynamic MR images. MRCP showed intrahepatic bile duct dilatation in all cases. Biliary hemorrhage was clearly depicted by MR images in five cases and showed hyperintensity on T1-weighted images and hyperintensity or hypointensity on T2-weighted images. Biliary hemorrhage was confirmed by endoscopy in two cases. Portal vein thrombi were also associated in five of six patients. Pathologically, tumor thrombi of HCCs were demonstrated in two patients who underwent hepatic resection. In conclusion, MR imaging is useful for the diagnosis of biliary tumor thrombi from HCC and for evaluating the extension of thrombi and biliary hemorrhage.

Key words: Hepatocellular carcinoma—Tumor thrombus—Liver—Bile duct—MR imaging

Jaundice is found in 19–40% of patients with hepatocellular carcinoma (HCC) [1]. The main causes of this complication are underlying cirrhosis, or extensive tumor invasion. Tumor thrombus in the intrahepatic bile duct by HCC is a rare cause of obstructive jaundice with incidence of 2–9% [2–4]. Several repots concerning HCCs with biliary tumor thrombi have been described. Cholangiographic findings during percutaneous transhepatic biliary drainage and CT findings were previously described [5, 6]. However, MR imaging features of biliary tumor thrombus of HCCs were reported only in one series [7]. Here we describe the MR and MR cholangiographic findings of HCCs with biliary tumor thrombi.

Materials and methods

The study group included four men and two women, 58–73 years of age (mean 64 years). Initial symptoms at admission included obstructive jaundice in all patients and melena due to biliary hemorrhage in three patients which was demonstrated by gastroendoscopy.

MR examinations

MR imaging was performed with a superconducting 1.5-T MR imager (Signa Horizon; GE Medical Systems, Milwaukee, WI, USA). Spin-echo (SE) T1-weighted images [TR 500 ms, TE 9 ms (500/9), two acquisitions, 256 × 192 matrix], and respiratory-triggered fast SE (FSE) T2-weighted images with the frequency selective fat-suppression technique [TR 3333-6666/80-90 (effective TR/effective TE), echo-train length of 8–12, 256 × 224 matrix, three acquisitions] were obtained. The slice thickness was 6 mm with a 2 mm intersection gap for T1- and T2-wighted images. Axial or oblique coronal dynamic MR imaging (SPGR, 160/1.6/90°, 256 × 128 matrix, one acquisition, fat suppression) with breath holding was performed.

Correspondence to: Toshifumi Gabata; *email:* gabata@med.m.kanazawa-u.ac.jp

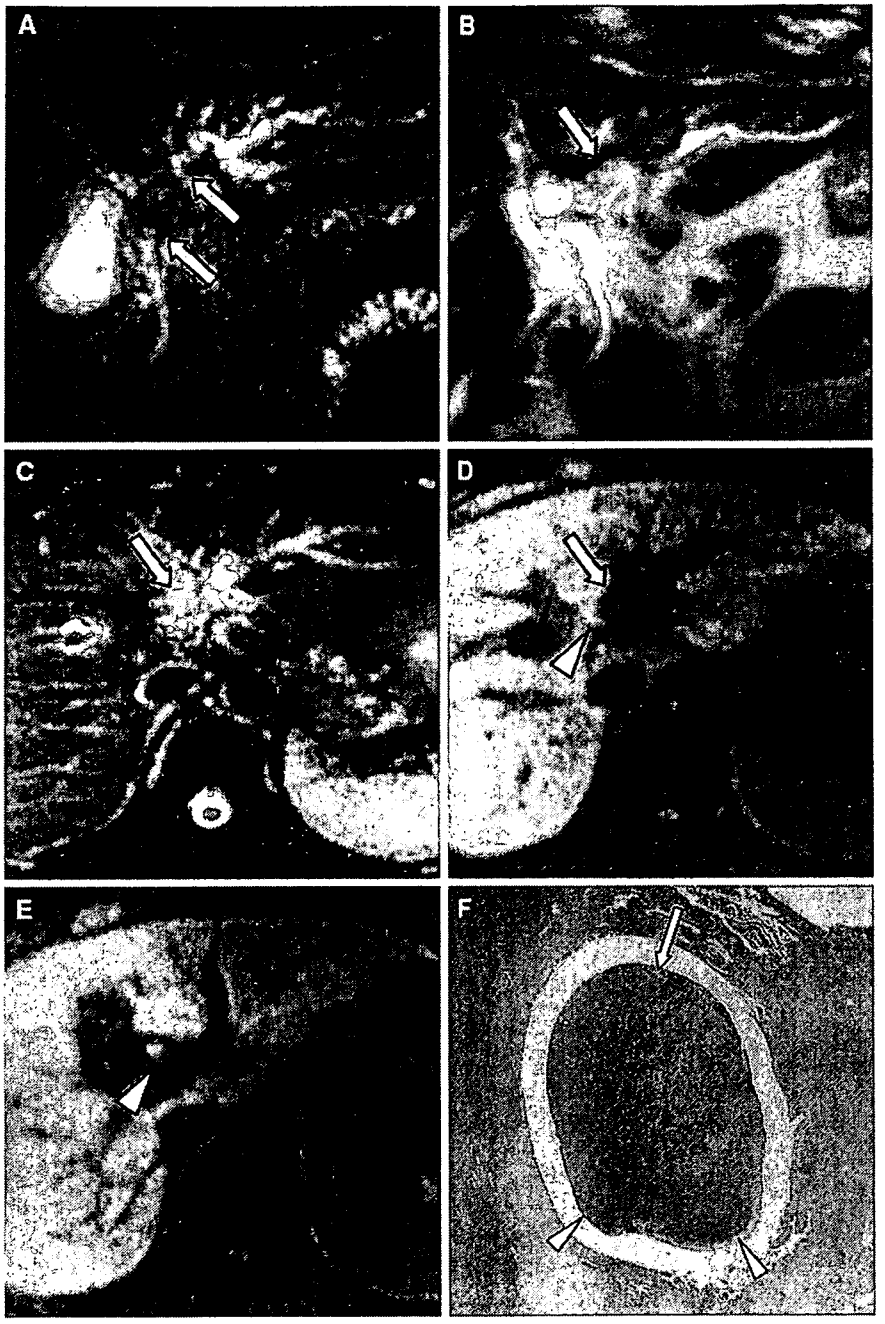

Fig. 1. 57-year-old man with HCC who presented jaundice and melena. **A** MR cholangiopancreatography (MRCP) shows filling defect of left hepatic duct and common hepatic duct (*arrow*) and intrahepatic bile duct dilatation of the left lateral segment of the liver. **B** Coronal T2-weighted image (single shot first spin echo) shows slightly hyperintense intrabiliary tumor thrombus in the left hepatic duct (*arrow*). **C** On axial T2-weighted image, the tumor thrombus shows hyperintensity (*arrow*). **D, E** On axial T1-weighted image (gradient echo), the tumor thrombus shows hypointensity (*arrow*), and dilated common hepatic duct shows hyperintensity indicating biliary hemorrhage (*arrowhead*). **F** Low power micrograph shows tumor thrombus (*arrow*) with hemorrhage (*arrowhead*) within the bile duct (**H, E**, ×2.5).

Dynamic MR imaging with SPGR sequence was acquired before and after intravenous administration of gadopentetate dimeglumine (Magnevist, Schering, Berlin, Germany). The slice thickness was 4–6 mm with 2 mm gap. MR cholangiopancreatography (MRCP) was also performed using a single shot first spin echo (SSFSE) sequence with a phased array coil. Both coronal thick slice MRCP (5 cm thick) using long TE (900 ms) and multislice MRCP images using medium TE (90 ms) in multiple oblique planes (4 mm thick, gapless) were obtained.

Results

Three HCCs were seen in the right lobe and the others were in the left lobe of the liver with 1.8–10 cm diameter (mean 5.8 cm). Biliary dilatation was visible in both lobes ($n = 3$), left lobe ($n = 2$), left lateral segment ($n = 1$), and posterior segment of the right lobe ($n = 1$). Biliary tumor thrombi were detected in all patients on MR imaging (Figs. 1, 2, 3). Tumor thrombi showed hypointensity on T1-weighted images, hyperintensity on T2-weighted images, and contrast enhancement in the

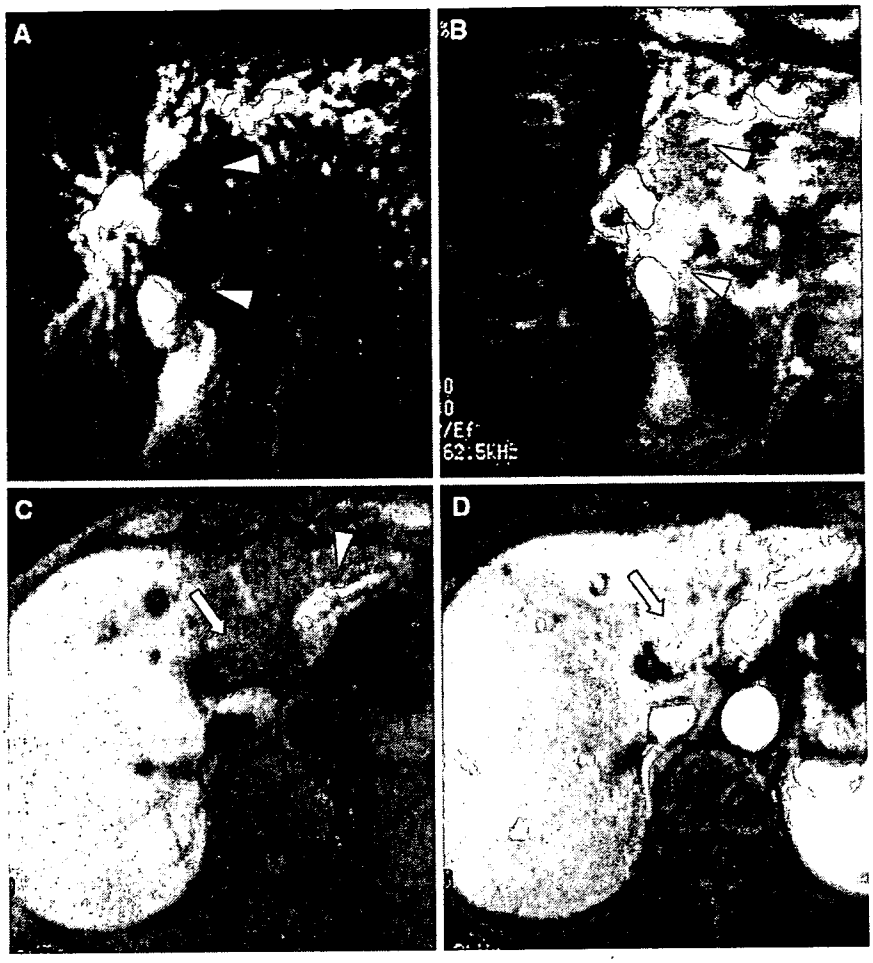

Fig. 2. 52-year-old man with HCC who presented jaundice. **A** MRCP shows filling defect of the left hepatic and common hepatic duct (*arrowhead*) and intrahepatic bile duct dilatation. **B** Coronal T2-weighted MR image (single shot first spin echo) shows hyperintense tumor thrombus (*arrowhead*). **C** On axial T1-weighted MR image (gradient echo), tumor thrombus shows hypointensity (*arrow*). The dilated left intrahepatic bile duct shows hyperintensity indicating biliary hemorrhage (*arrowhead*). **D** Arterial dominant phase of dynamic MR image (gradient echo) shows marked enhancement of the tumor thrombus with segmental enhancement of the lateral segment of the liver due to invasion of the left portal vein by HCC (not shown).

early phase of dynamic MR images. MRCP showed intrahepatic bile duct dilatation in all cases. Tumor thrombus was depicted as a filling defect on MRCP, whereas coronal SSFSE T2-weighted images showed biliary dilatation and the tumor thrombus itself. Biliary hemorrhage was clearly depicted by MR images in five cases which showed hyperintensity on T1-weighted images and hyperintensity or hypointensity on T2-weighted images. Biliary hemorrhage was confirmed by endoscopy in two cases. Portal vein thrombi were also associated in five of six patients. Pathologically, tumor thrombi of HCC were demonstrated in two patients who underwent hepatic resection.

Discussion

Although invasion of the portal vein or hepatic vein is commonly seen in HCC, invasion of the intrahepatic bile duct is quite rare. Kojiro et al. [2] described 24 cases (9%) of HCC with bile duct tumor thrombus in 259 cases (238 autopsy, 21 surgical). Ikeda et al. [3] reported 13 (5.1%) of 257 patients with HCC with intrabiliary tumor growth, intrahepatic metastases, and portal vein invasion. Patients with biliary tumor thrombi with HCC with intrabiliary tumor growth, intrahepatic metastases, and portal vein invasion. Patients with biliary tumor thrombi with HCC show obstructive jaundice or melena due to biliary hemorrhage. Despite recent advances in diagnostic modalities of HCC, patients with biliary tumor thrombus of HCC are frequently misdiagnosed with biliary choledocholithiasis or bile duct carcinoma. Patients with bile duct tumor thrombus frequently have hemobilia from bleeding of the advanced portion of HCC. If the main extrahepatic bile duct is occluded, obstructive jaundice is clinically evident. The causes of obstruction of the bile duct include direct blockage of the common hepatic duct of the tumor itself, blood clot from the tumor, and tumor fragment [3]. Fresh hemorrhage within the intrahepatic and extrahepatic bile duct may mimic choledocholithiasis and obscure the tumor itself on precontrast CT. So, dynamic contrast enhanced CT is necessary to detect HCC and differentiate it from tumor within the bile duct and hemorrhage. Because subacute hemorrhage does not show hyperdensity but isodensity or hypoden-

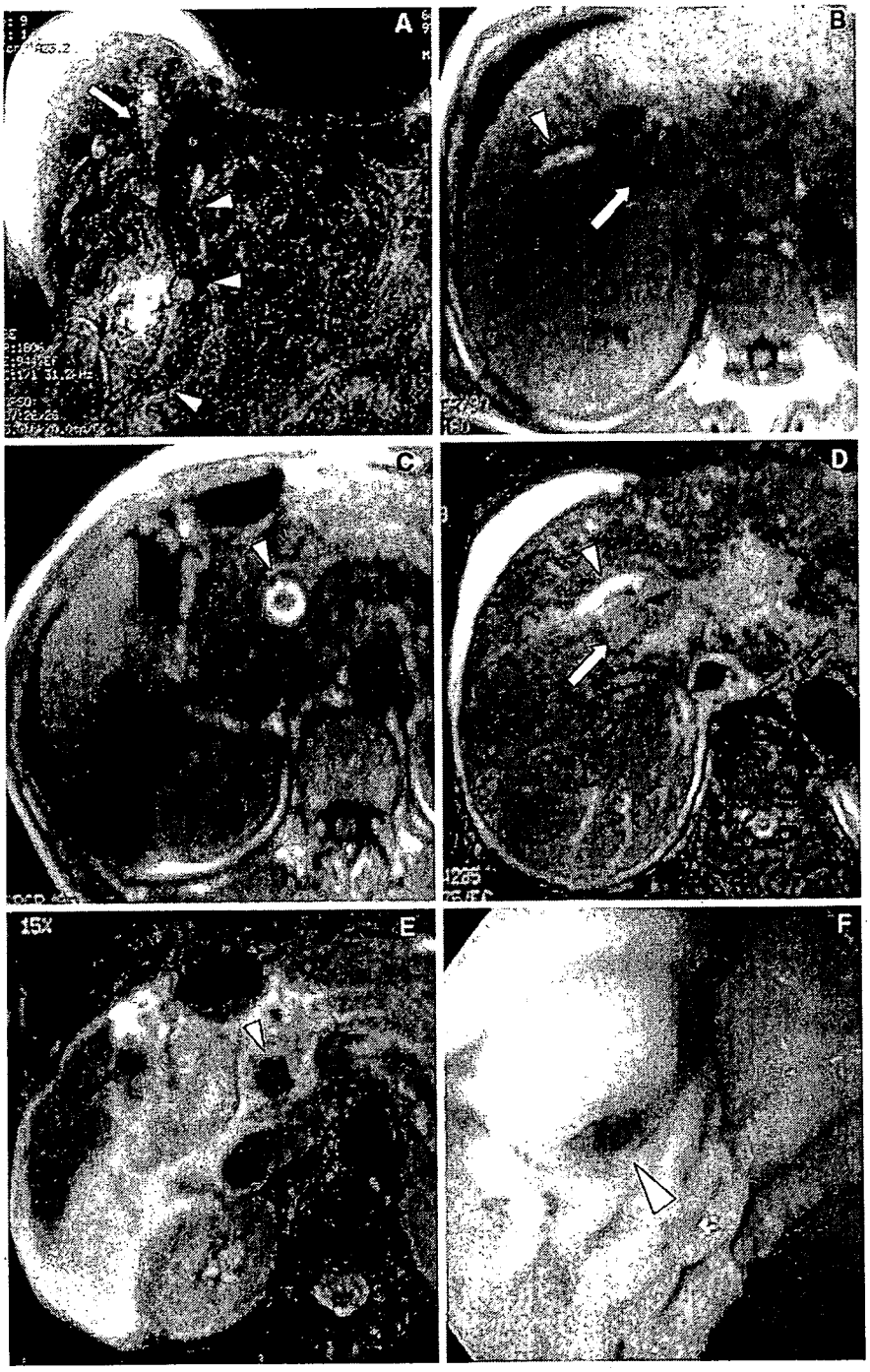

Fig. 3. 66-year-old woman with HCC who presented jaundice and melena. **A** MRCP shows dilated intrahepatic bile duct of the right lobe of the liver (*arrow*). The dilated extrahepatic bile duct shows hypointensity due to subacute hemorrhage. The tip of the drainage balloon catheter is visible within the common bile duct. **B, C** T1-weighted MR images show hypointense tumor thrombus of the right hepatic duct (**B**, *arrow*). The dilated right anterior superior bile duct (**B**, *arrowhead*) and common bile duct (**C**, *arrowhead*) show hyperintensity due to hemorrhage. **D, E** On T2-weighted MR images, tumor thrombus and dilated intrahepatic duct show hyperintensity, while dilated common bile duct shows hypointensity due to subacute hemorrhage. (**E**, *arrowhead*), **F** Duodenal endoscopy shows active bleeding from the dilated papilla of Vater (*arrowhead*).

sity on precontrast CT without contrast enhancement, we cannot differentiate between subacute hemorrhage and necrotic tumor. MR imaging is useful for detection of tumor thrombus of the bile duct. In our cases, tumor thrombi of bile duct showed hypointensity on T1-weighted images and hyperintensity on T2-weighted images and contrast enhancement in the early phase of dynamic MR images. MR imaging also clearly differentiated tumor thrombus from intrabiliary hemorrhage which shows hyperintensity on T1-weighted images, hyperintensity or hypointensity on T2-weighted images without contrast enhancement on dynamic MR images. MRCP can depict intrahepatic bile duct dilatation and the extent of biliary obstruction; however, tumor thrombi and hemorrhage cannot be discriminated. Multislice MRCP images using medium TE (90 ms) are useful in the discrimination of tumor thrombus and intrabiliary hemorrhage based on their signal intensity difference.

In conclusion, MR imaging is useful for the diagnosis of biliary tumor thrombi from HCCs and for evaluating the extension of thrombi and biliary hemorrhage.

References

1. Wang HJ, Kim JH, Kim JH, et al. (1999) Hepatocellular carcinoma with tumor thrombi in the bile duct. Hepatogastroenterology 46(28):2495–2499
2. Kojiro M, Kawabata K, Kawano Y, et al. (1982) Hepatocellular carcinoma presenting as intrabile duct tumor growth: a clinicopathologic study of 24 cases. Cancer 49:2144–2147
3. Ikeda Y, Matsumata T, Adachi E, et al. (1997) Hepatocellular carcinoma of the intrabiliary growth type. Int Surg 82:76–78
4. Satoh S, Ikai I, Honda G, et al. (2000) Clinicopathologic evaluation of hepatocellular carcinoma with bile duct thrombi. Surgery 128:779–783
5. Chen MF, Jan YY, Jeng LB, et al. (1994) Obstructive jaundice secondary to ruptured hepatocellular carcinoma into the common bile duct. Cancer 73:1335–1340
6. Soyer P, Sibert A, Laissy JP (1995) Intrahepatic bile duct dilatation secondary to hepatocellular carcinoma: CT features in 10 patients. Abdom Imaging 20:114–117
7. Soyer P, Laissy JP, Bluemke DA, et al. (1995) Bile duct involvement in hepatocellular carcinoma: MR demonstration. Abdom Imaging 20:118–121